Bioresource Technology 287 (2019) 121418

Contents lists available at ScienceDirect

Bioresource Technology

journal homepage: www.elsevier.com/locate/biortech

Applying the electrode potential slope method as a tool to quantitatively evaluate the performance of individual microbial electrolysis cell components

Benjamin P. Cario[a], Ruggero Rossi[a], Kyoung-Yeol Kim[b], Bruce E. Logan[a,*]

[a] Department of Civil and Environmental Engineering, The Pennsylvania State University, 231Q Sackett Building, University Park, PA 16802, USA
[b] Department of Environmental and Sustainable Engineering, University at Albany, State University of New York, 1400 Washington Avenue, Albany, NY 12222, USA

ARTICLE INFO

Keywords:
Bioelectrochemical system
Microbial electrolysis cell
Internal resistance
Electrode potential slope method
Felt anode

ABSTRACT

Improving the design of microbial electrolysis cells (MECs) requires better identification of the specific factors that limit performance. The contributions of the electrodes, solution, and membrane to internal resistance were quantified here using the newly-developed electrode potential slope (EPS) method. The largest portion of total internal resistance (120 ± 0 mΩ m^2) was associated with the carbon felt anode (71 ± 5 mΩ m^2, 59% of total), likely due to substrate and ion mass transfer limitations arising from stagnant fluid conditions and placement of the electrode against the anion exchange membrane. The anode resistance was followed by the solution (25 mΩ m^2) and cathode (18 ± 2 mΩ m^2) resistances, and a negligible membrane resistance. Wide adoption and application of the EPS method will enable direct comparison between the performance of the components of MECs with different solution characteristics, electrode size and spacing, reactor architecture, and operating conditions.

1. Introduction

Microbial electrolysis cells (MECs) are a type of bioelectrochemical system (BES) used to simultaneously treat organic waste streams and sustainably produce hydrogen gas. These technologies have a wide range of potential applications, including incorporation into wastewater treatment (Cotterill et al., 2018, Jwa et al., 2019, Roubaud et al., 2018, Aiken et al., 2019), anaerobic digestion (Yu et al., 2018, Hassanein et al., 2017), and the processing of lignocellulosic biomass (Wang et al., 2017, Wang et al., 2011, Lalaurette et al., 2009). Under typical MEC solution conditions, a small voltage addition is required to drive current production and hydrogen evolution (Liu et al. 2005). The internal resistance of an MEC impacts how much current is produced at a given applied voltage, with lower resistance corresponding to higher current. Therefore, minimizing the internal resistance of a reactor maximizes its electrical efficiency, and should be a key consideration during system design. Although total internal resistance is what determines electrical efficiency, breaking the total resistance into individual component resistances, such as the resistance associated with each electrode, can assist in analyzing system performance. Previous research has shown that component-associated losses are impacted by design choices such as electrode and membrane materials, solution conductivity, pH, reactor configuration, electrode size, and hydrodynamic conditions (Sleutels et al., 2009b, Logan et al., 2018, Rozendal et al., 2006, Sleutels et al., 2009a, Rozendal et al., 2007, Jeremiasse et al., 2010, Miller et al., 2019). Unfortunately, nearly all of the methodologies used in past studies do not indicate the extent to which these elements affect performance across a range of reactor types and operating conditions. While conclusions regarding a single set of conditions can help identify methods to improve performance, more quantitative and consistent approaches are needed to facilitate inter-study comparisons and identify the most important factors that limit BES performance.

In past MEC research, performance has most often been compared on the basis of maximum current densities and hydrogen production rates (Jwa et al., 2019, Wang et al., 2017, Nam and Logan, 2012, Jayabalan et al., 2018, Rago et al., 2016, Wang and Ren, 2013, Belleville et al., 2018, Guo and Kim, 2018). This analysis is useful for determining how one factor, such as the cathode material, can impact performance relative to a control, but it does not allow for comparison between studies with other differences (such as anode materials, electrode spacing, electrode size). Linear sweep voltammetry and chronopotentiometry have been used to isolate performance of the cathode (Kim et al., 2018, Li et al., 2017, Kim et al., 2017, Choi et al., 2019), but

* Corresponding author.
E-mail address: blogan@psu.edu (B.E. Logan).

https://doi.org/10.1016/j.biortech.2019.121418
Received 27 March 2019; Received in revised form 1 May 2019; Accepted 2 May 2019
Available online 04 May 2019
0960-8524/

these methods do not provide insight as to the relative impact of the anode, reactor configuration, and solution conditions on overall performance. Evaluation of component-associated internal losses provides a more complete analysis of system performance than most common methods. Occasionally, MEC internal losses have been examined on the basis of voltage (Rozendal et al., 2006, 2007, Jeremiasse et al., 2010), but the magnitudes of voltage losses are a function of the applied voltage, the external resistance, and the current in the circuit. Thus, voltage loss analysis does not allow for direct comparison between systems with different applied voltages or current densities. Based on Ohm's Law, internal voltage losses can be divided by current to obtain total and component-associated internal resistances. Because internal resistance values are independent of applied voltage and current over a wide range of typical operating conditions, they facilitate more accurate analysis and better interstudy comparison than voltage losses. However, internal resistance values may change at very low or very high current densities if activation losses or substrate limitations occur. Therefore, examining internal resistance data from a single applied voltage, as has been done in several previous MEC studies (Sleutels et al., 2009a,b), may not accurately describe total and component-associated internal resistances under all possible conditions. MEC internal resistance values obtained over a range of applied voltages have only been reported in one prior study (Miller et al., 2019), where component-associated resistances were calculated using a non-linear least-squares algorithm and whole-cell data.

It is shown here that the performance of MEC components (anode, cathode, solution, and membrane) can be directly quantified and compared on the basis of area-normalized resistances using the electrode potential slope (EPS) method, which was recently developed for the analysis of microbial fuel cells (MFCs) (Rossi et al., 2019). To use this method, polarization data must be obtained for each electrode and the whole cell over a range of current densities, and measurements must be made on the solution conductivity, the distance between the electrodes, and the cross-sectional area between the electrodes, or if present, the membrane. Based on the slopes of the polarization data, area-normalized resistances can be calculated for the whole cell and each electrode and compared to those of the solution (from conductivity measurements) and the membrane (by difference using the whole-cell, solution, and individual electrode resistances). By expressing resistances on the basis of area, it is possible to directly and quantitatively compare component-associated resistances between studies using different electrode materials, size, orientation, and spacing. It is also possible to more thoroughly evaluate the impact of operating conditions and solution characteristics on performance. The utility of this method was demonstrated here using cube-type MECs, which have the same general structure as those used in previous studies of hydrogen production using MECs (Kim et al., 2018, Nam and Logan, 2012, Zikmund et al., 2018, Call and Logan, 2008, Ambler and Logan, 2011, Call et al., 2009) and electricity production using MFCs (Yang et al., 2017).

2. Materials and methods

2.1. Electrode potential slope method

The theoretical change in voltage across an electrochemical cell (E_{cell}) is the difference between the cathode potential (E_{cat}) and the anode potential (E_{an}), or:

$$E_{cell} = E_{cat} - E_{an} \quad (1)$$

Assuming complete oxidation of acetate to carbon dioxide at the anode, hydrogen gas evolution from protons at the cathode, and standard biological conditions (pH = 7, 298 K, 1 M concentrations of all reactants and products, 1 atm H_2 and CO_2), the calculated cell voltage for microbial electrolysis is E_{cell} = (–0.42 V) – (–0.28 V) = –0.14 V (Rozendal et al., 2006, Ullery and Logan, 2015). Thus, an applied voltage of ≥0.14 V is required to thermodynamically drive an MEC under these solution conditions. For real systems, irreversible internal and external losses must also be taken into account. In practice, voltages greater than 0.5 V are generally applied to an MEC circuit (Sleutels et al., 2009b, Rozendal et al., 2006, Sleutels et al., 2009a, Rozendal et al., 2007, Jeremiasse et al., 2010). When losses are considered, the governing equations become:

$$E_{ap} = |E_{cell,m} - IR_{ext}| \quad (2)$$

$$E_{cell,m} = E_{cell,e0} - IR_{int} = E_{cat,e0} - E_{an,e0} - IR_{int} \quad (3)$$

where E_{ap} is the applied voltage (mV), $E_{cell,m}$ is the measured voltage drop over the cell (mV), I is area-normalized current density (A/m^2), R_{ext} is the external resistance in the circuit (mΩ m^2), and R_{int} is the sum of all internal resistances in the cell (mΩ m^2). Measured voltage drop over the cell ($E_{cell,m}$) will be more negative than E_{cell} as defined in Eq. (1) because of internal losses, as shown in Eq. (3). Whole-cell and electrode potentials measured at a range of applied voltages can be plotted as a function of current density to obtain polarization curves. Polarization data can contain three characteristic regions: a non-linear change in potential due to activation losses at low current densities, a linear range due to ohmic losses over most of the useful range of current densities, and a rapid change in potential due to concentration (mass transfer) limitations at high current densities (Logan, 2008). Experimental open circuit potentials for the whole cell ($E_{cell,e0}$), the cathode ($E_{cat,e0}$), and the anode ($E_{an,e0}$), can be directly obtained from the y-intercepts of the fits of the linear portions of the polarization data, and activation losses (η_{cell}, η_{cat}, η_{an}) can be calculated as the difference between the experimental open circuit potentials and theoretical values (Fig. 1, except as otherwise noted below). Using $E_{cell,e0}$, $E_{cat,e0}$, and $E_{an,e0}$ for analysis instead of theoretical potentials based on half-cell reactions is different than previous approaches applied to MECs (Sleutels et al., 2009b, Rozendal et al., 2006, Sleutels et al., 2009a, Jeremiasse et al., 2010). The equations presented here are modified slightly from the EPS analysis for MFCs due to the inclusion of the applied voltage in Eq. (2).

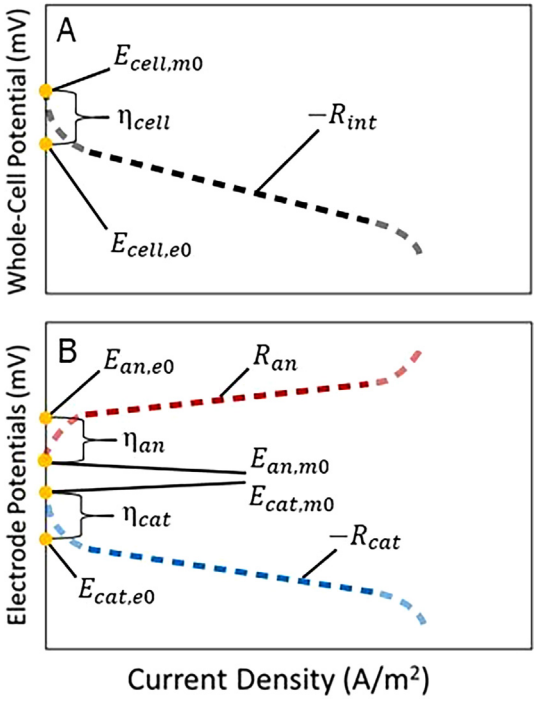

Fig. 1. Analysis of polarization data using the electrode potential slope (EPS) method for (A) the whole cell, and (B) the individual electrodes. Non-linear activation losses (low current, light dashed lines) or rapid changes in voltage (high current) are not used in the analysis, which only includes the linear range (ohmic-loss region) of the polarization curves (dark dashed lines).

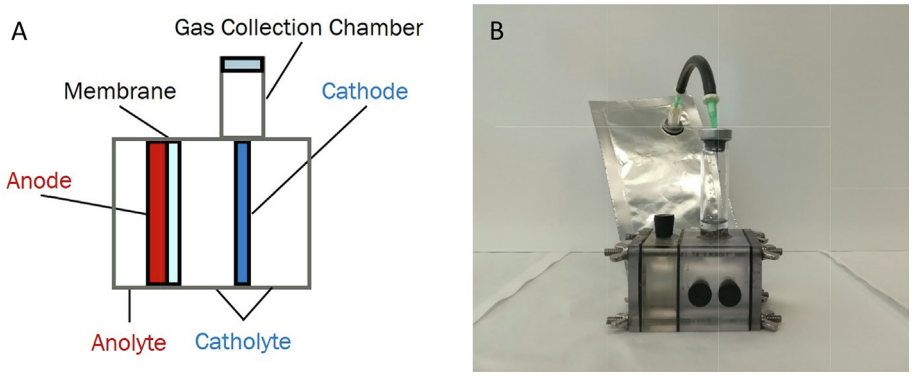

Fig. 2. Two-chamber microbial electrolysis cell with a felt anode and platinum-catalyzed stainless steel mesh cathode: (A) schematic (not to scale), and (B) photograph, also showing the gas collection bag attached to the gas collection chamber.

The measured open circuit or electrode potentials for MFCs (E with a subscript $m0$) also do not have exact counterparts here due to the need for an applied voltage with MECs. However, the equivalent "measured" open circuit cell and electrode potentials ($E_{cell,m0}$, $E_{an,m0}$, and $E_{cat,m0}$) could be obtained by using a high external resistance in the circuit.

The internal resistance of an MEC can be further separated into individual components:

$$R_{int} = R_{cat} + R_{an} + R_{\Omega} + R_{mem} \quad (4)$$

$$E_{cell,m} = E_{cat,m} - E_{an,m} - I(R_{\Omega} + R_{mem}) \quad (5)$$

$$E_{cat,m} = E_{cat,e0} - IR_{cat} \quad (6)$$

$$E_{an,m} = E_{an,e0} + IR_{an} \quad (7)$$

$$R_{\Omega} = \frac{100 d_{mem-cat}}{\sigma} \quad (8)$$

where R_{cat} is the cathode resistance (mΩ m^2), R_{an} is the anode resistance (mΩ m^2), R_{Ω} is the ohmic resistance of the solution (mΩ m^2), R_{mem} is the membrane resistance in two-chamber systems (mΩ m^2), $E_{cat,m}$ is the measured cathode potential (mV), $E_{an,m}$ is the measured anode potential (mV), $d_{mem-cat}$ is the distance between the membrane and the cathode (cm), σ is the catholyte conductivity (mS/cm), and 100 is a unit conversion factor. If the reference electrodes used to measure cell electrode potentials are within the current path, the measured cell electrode potentials must be corrected for ohmic resistance between the cell electrodes and the reference electrodes, as previously described by Logan et al. (Logan et al., 2018, Zhang et al., 2014). When trendlines are fit to the linear portions of whole-cell and electrode polarization data, the slopes can be used to directly estimate total and electrode-associated resistances using Eqs. (3, 6, 7) (Fig. 1). Solution resistance can be calculated using Eq. (8), allowing membrane resistance to be computed as the sole unknown in Eq. (4). Plotting area-normalized current density on the horizontal axis of the polarization curves generates internal resistance values in units of mΩ m^2. Since large systems generally produce more total current than small systems at a given applied voltage, they have lower internal resistances in units of mΩ. However, when internal resistances are normalized by cross-sectional area, larger systems tend to have higher specific resistances in units of mΩ m^2. Using the area-normalized unit better reflects the trend of efficiency loss with reactor scale-up and allows for direct comparison between reactors of different size. In contrast to previous studies by Rozendal et al. (2007) and Sleutels et al. (2009a), there is no term to account for pH-associated losses in our analysis. The impacts of pH and mass transport at the electrodes are already included in the measured electrode potentials and therefore a separate term is not needed.

If the linear fit of the experimental data spans the region of the polarization curve where ohmic losses are dominant, the experimental open circuit potential will differ from the "measured" open circuit potential by the magnitude of the activation losses, as noted above (Fig. 1). Polarization data for BESs tend to be linear over nearly the whole range of current densities, indicating that these systems generally operate at current densities where ohmic losses are dominant. However, if the linear fit of the data spans the activation loss region of the polarization curve, the computed experimental open circuit potential could equal the "measured" open circuit potential, and the calculated resistance will include the impact of activation losses. Therefore, it is important to consider what region(s) of the polarization curve are represented by the data when using the EPS analysis. In this study, "measured" open circuit potentials (which were not critical to our analysis) were estimated using theoretical half-cell reactions under standard biological solution conditions, but theoretical values may differ from "measured" values due to side reactions at the electrodes and/or non-standard solution conditions during operation.

2.2. Reactor configuration

Two MECs (duplicates, Fig. 2) were constructed from blocks of polycarbonate drilled to have a 14 mL anode chamber (radius of 1.5 cm, length of 2 cm) and a 28 mL cathode chamber (radius of 1.5 cm, length of 4 cm), which were separated by an anion exchange membrane (AEM, Selemion AMV, AGC Engineering Co. Ltd., JP). A 6.35 mm-thick carbon felt anode (Alfa Aesar, MA) was placed against the membrane, in contact with a titanium current collector. The cathode was constructed from stainless steel mesh, treated with a platinum/carbon mixture (ETEK C1-10, 10% Pt and Vulcan XC-72) and a Nafion binder (5 wt% solution, Aldrich Nafion® perfluorinated ion-exchange resin), as previously described (Nam and Logan, 2012). The electrode was suspended in the cathode chamber, 1.5 cm from the AEM. Both electrodes and the membrane shared the cross-sectional area of the reactor (7 cm^2). A stoppered glass tube extended from the top of the cathode chamber and was connected via a needle and tubing to a gas collection bag (Cali-5-Bond, Calibrated Instruments, NY). Two Ag/AgCl reference electrodes (+200 mV vs. SHE) were placed in each reactor, one in the anode chamber (1 cm from the anode) and one in the cathode chamber (1.5 cm from the cathode).

2.3. Operation

MECs were operated in batch-fed mode in a constant temperature room (30 °C) with a voltage of 0.9 V applied using a DC power supply (B &K Precision, CA), except as noted. The catholyte was a 50 mM phosphate buffer solution (PBS, 4.58 g/L Na_2HPO_4, 2.45 g/L NaH_2PO_4, 0.31 g/L NH_4Cl, 0.13 g/L KCl, pH = 7.12, conductivity = 5.96 mS/cm). MEC anodes were initially inoculated with primary clarifier effluent from the Pennsylvania State University Wastewater Treatment Plant and acclimated to a synthetic fermentation effluent (0.27 g/L sodium acetate, 0.11 g/L ethanol, 0.07 g/L lactic acid, 0.15 g/L glucose, 0.32 g/

L bovine serum albumin, in 50 mM PBS, trace vitamins and minerals, pH = 7.12, conductivity = 8.13 mS/cm). After operation for several months with synthetic fermentation effluent, they were switched to medium containing 1.5 g/L sodium acetate (50 mM PBS, trace vitamins and minerals, pH = 7.22, conductivity = 6.49 mS/cm). Prior to the tests reported here, they were considered fully acclimated after demonstrating three reproducible current cycles.

2.4. Measurements and calculations

A 10 Ω external resistor was placed between the power supply and the anode in each circuit, and the voltage drop across the resistor was measured every 20 min using a multimeter (Model 2700, Keithley Instruments, Inc., OH) to calculate current using Ohm's Law. Current densities were normalized by membrane cross-sectional area (7 cm^2). The multimeter was also used to record the individual electrode potentials (vs. Ag/AgCl, reported vs. SHE) and the voltage drop over the cell. The measured cell electrode potentials were not corrected for solution resistance between the reference electrodes and cell electrodes since the reference electrodes were outside of the current path (Zhang et al., 2014). Conductivity and pH measurements were taken with a conventional conductivity meter and pH probe (Seven-Multi, Mettler-Toledo International Inc).

To obtain polarization data, the applied voltage was reduced from 0.9 V to 0.2 V at 0.1 V intervals over multiple cycles. A minimum of three reproducible current cycles were obtained at each applied voltage. Five points around peak current were averaged to obtain a representative value for current, cell voltage drop, anode potential, and cathode potential from each cycle. Representative values obtained from reproducible cycles were then averaged to acquire a single data point for each parameter at a given applied voltage. These data points were used to produce whole-cell and electrode polarization curves. Trendlines were fit to the linear portions of the polarization curves, and the components of internal resistance were quantified using the EPS method, as outlined above.

3. Results and discussion

Whole-cell and electrode polarization data were highly linear ($R^2 \geq 0.95$) over the current density range up to ~5 A/m^2, with activation losses having no obvious impact on the relationship between current and potential at low current densities (Fig. 3a). Thus, most data were in the linear ohmic loss region of the polarization curves. There was a sudden rise in the anode potentials at the highest current densities (0.8–0.9 V applied), which caused a corresponding drop in the whole-cell potentials. Therefore, increasing the applied voltage beyond 0.8 V did not increase current production and reduced electrical efficiency (Fig. 3). The non-linear response may have been caused by limited substrate availability and/or restrictive bacterial kinetics at the anode. Because the high-current data points fell outside of the linear portion of the polarization curves, they were not used in the anode or whole-cell EPS analyses.

3.1. Area-based resistances

The total internal resistance of the cube MECs was calculated to be R_{int} = 120 ± 0 mΩ m^2 from the linear portion of the whole-cell polarization curve (Fig. 3a). Based on the individual electrode data, the anode was the largest source of resistance in the system at R_{an} = 71 ± 5 mΩ m^2, with the cathode contributing 75% less resistance (R_{cat} = 18 ± 2 mΩ m^2) (Fig. 3b). The solution resistance was calculated as R_{Ω} = 25 mΩ m^2 using Eq. (8) and the experimental conditions ($d_{mem\text{-}cat}$ = 1.5 cm, σ = 5.96 mS/cm, R_{Ω} = 100 (1.5 cm)/(5.96 mS/cm)). The membrane was responsible for only a small portion of the total resistance, with R_{mem} = 6 ± 5 mΩ m^2 based on Eq. (4) and the other estimated resistance values (R_{mem} = 120 ± 0 mΩ m^2 – 71 ± 5 mΩ m^2 – 18 ± 2 mΩ m^2 – 25 mΩ m^2).

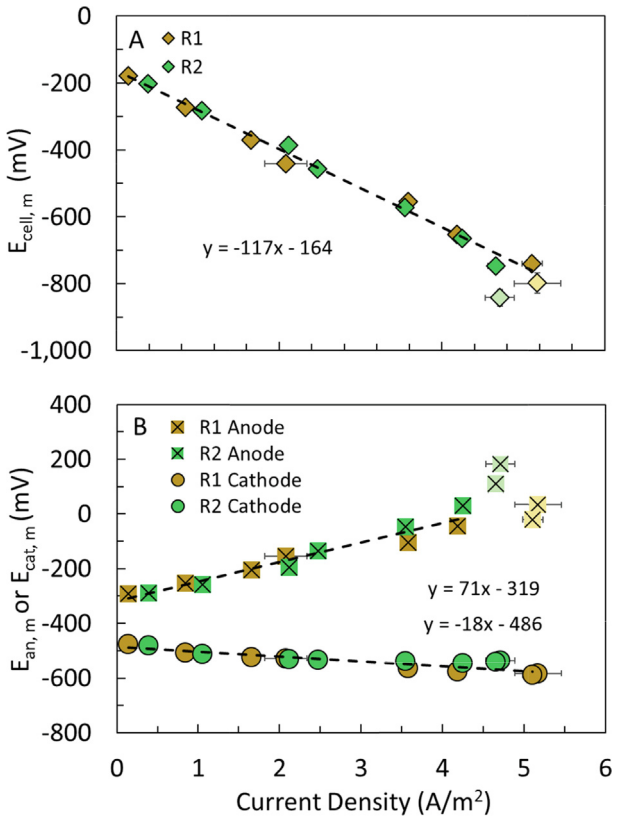

Fig. 3. (A) Whole-cell and (B) individual electrode polarization curves for acetate-fed cube MECs. R1 and R2 refer to duplicate reactors 1 and 2. Faded data points were not included in the linear fits.

The anode contributed the largest portion of the total internal resistance among individual components (R_{an} = 71 ± 5 mΩ m^2, 59%), indicating that it was the main factor limiting MEC performance. In past research on BESs, the cathode has most often been indicated as the primary current-limiting element (Rossi et al., 2019, Yang and Logan, 2016, Cheng and Logan, 2011, Watson et al., 2013). However, in several studies it has been reported that other factors were the main limitation, such as the anode or the presence of pH gradients (Sleutels et al., 2009a, Rozendal et al., 2007, Jeremiasse et al., 2010, Miller et al., 2019). A quantitative comparison between the electrode resistances determined here and previous studies can only be made in a few cases, as methodologies for analysis have varied and often the data needed for EPS analysis has not been reported. In MFC tests using single-chamber cube reactors and a feed solution containing 1 g/L sodium acetate, anode resistance was 19 mΩ m^2 for a felt anode placed distant (3.1 cm) from the cathode (Logan et al., 2018), and 10.6 ± 0.5 mΩ m^2 for a brush anode placed 1 cm from the cathode (Rossi et al., 2019). These are both quite less than the anode resistance obtained here, indicating that using a brush anode can improve electrochemical performance and increase hydrogen gas production. The higher flat anode resistance obtained in this study was likely due to a combination of biofilm substrate limitations and poor ion transfer throughout the system. Mixing the electrolyte with a stir bar in batch-fed cube reactors (Miller et al., 2019, Zikmund et al., 2018) or using high electrolyte flow rate in continuous flow systems (Jafary et al., 2017, Cario, 2019) has previously been shown to enhance the performance of flat-anode BESs by improving mass transfer to and from the biofilm. Recently, the resistance associated with a carbon cloth anode in a single-chamber, acetate-fed MEC was found to decrease from 21 mΩ m^2 to 15 mΩ m^2 when the feed solution was "shaken", while small changes in electrode spacing did not impact performance (Miller et al., 2019). Forcing

anolyte to flow through the electrode may also improve mass transfer, as a prior MEC study found the resistance of a 1 mm-thick felt anode with forced flow to be just 20 mΩ m^2 (1.5 g/L acetate, based on only one data point) (Sleutels et al., 2009b).

In addition to hydrodynamic conditions (flow versus no-flow), placement of the anode can also impact reactor performance. Pressing the anode against the membrane, as was done in this study, may increase internal resistance by physically hindering the ion transfer needed for charge balance between the anolyte and catholyte (Sleutels et al., 2009b). Furthermore, placing the anode against the membrane causes most of the anolyte to be outside of the electric field, and thus negatively-charged buffers and substrates (like the phosphate and acetate ions in this study) are not pulled toward the biofilm as they would be if the anode was on the far side of the chamber and the anolyte was between the electrodes (Marcus et al., 2010, Torres et al., 2008, Ahn et al., 2014). The main disadvantage of moving the anode distant from the membrane is the addition of anolyte solution resistance to the total internal resistance. It was assumed here that there was no anolyte resistance since the anode and membrane were pressed together. However, if the anode had been placed 3 cm from the membrane as was done in past MFC studies, an additional 46 mΩ m^2 of resistance would have been introduced based on the low electrolyte conductivity (σ = 6.49 mS/cm) and Eq. (8) (R_Ω = 100 (3 cm)/(6.49 mS/cm)). Therefore, it can be estimated that the combined anode and anolyte resistance would have been 65 mΩ m^2 if the anode was 3 cm from the membrane (using the 19 mΩ m^2 anode resistance from the MFC study and 46 mΩ m^2 for the anolyte resistance). That is only slightly less than the 71 mΩ m^2 obtained here with the anode against the membrane. In this way, the EPS method can help guide the assessment of anode placement in future studies.

3.2. Whole-cell and electrode potentials

The experimental open circuit cell voltage drop was $E_{cell,e0}$ = –160 ± 10 mV based on the *y*-intercept of the whole-cell polarization curve and Eq. (3) (Fig. 3a). This translated to a whole-cell activation loss of η_{cell} = 20 ± 10 mV when compared to the assumed standard biological conditions (–140 mV). The experimental open circuit electrode potentials were $E_{cat,e0}$ = –490 ± 10 mV for the cathode and $E_{an,e0}$ = –320 ± 20 mV for the anode based on the *y*-intercepts of the electrode polarization curves (Fig. 3b). The difference between the experimental open circuit electrode potentials ($E_{cat,e0}$ – $E_{an,e0}$ = –170 ± 20 mV) was comparable to that of the experimental whole-cell potential under open circuit conditions ($E_{cell,e0}$ = –160 ± 10 mV, Eq. (3)).

Comparing the experimental open circuit electrode potentials to those calculated using half-cell potentials under standard biological conditions (E_{an} = –280 mV, E_{cat} = –420 mV) showed activation losses of η_{an} = –40 ± 20 mV for the anode and η_{cat} = 70 ± 10 mV for the cathode. The negative anode activation loss could have been due to several factors. First, linear regression of the data showed that the error in the *y*-intercept was ± 20 mV (overall R^2 = 0.95, with a standard error of the slope = 7%), so a portion of this difference could have been due to the accuracy of the linear fit. A second factor in the difference between the experimental and theoretical half-cell potentials could have been differences between standard biological conditions and the actual conditions in the solution. For example, all solution concentrations were assumed to be 1 M under standard conditions. While the theoretical potentials could have been adjusted for the actual acetate concentration added into the MEC, the concentration of HCO_3^- in solution near the electrode could not be easily measured. Of these two explanations, the second seems more likely since the sum of the electrode activation losses (η_{cat} + η_{an} = 30 mV) was approximately equal to the whole-cell activation loss (η_{cell} = 20 mV), and the whole-cell loss was also computed using the theoretical anode potential. In general, polarization data reported for anodes in both MECs and MFCs fed acetate have been quite linear, with previously-reported *y*-intercepts of –260, –262, and –290 mV (Rossi et al., 2019, Zikmund et al., 2018). Thus, the values obtained here are comparable to past studies. Similarly, abiotic half-cell chronopotentiometry conducted in 50 mM PBS has shown notable cathode activation losses for Pt/C-catalyzed hydrogen evolution, consistent with the findings of this study (Kim et al., 2018).

4. Conclusions

A carbon felt anode was the largest contributor to internal resistance in acetate-fed MECs (59% of total), followed by ohmic solution resistance (21%) and cathode resistance (15%). The high anode resistance was likely due to poor substrate and ion transport to bacteria on the anode and obstruction of ion transport through the AEM. The ability to diagnose system performance at the component-level and identify areas for improvement is a major strength of the newly-developed EPS method. Applying the procedure in future MEC research can facilitate more useful findings and, ultimately, more efficient hydrogen production from reduced waste streams.

Acknowledgements

This work was conducted at the Pennsylvania State University and supported by funds provided by the US Department of Energy (DOE) Energy Efficiency and Renewable Energy (EERE) Fuel Cell Technologies Office, through a contract from the National Renewable Energy Laboratory (NREL), Project #21263.

Appendix A. Supplementary data

Supplementary data to this article can be found online at https://doi.org/10.1016/j.biortech.2019.121418.

References

Ahn, Y., Hatzell, M.C., Zhang, F., Logan, B.E., 249 2014. Different electrode configurations to optimize performance of multielectrode microbial fuel cells for generating power or treating domestic wastewater. J. Power Sources 440, 5.
Aiken, D.C., Curtis, T.P., Heidrich, E.S., 2019. Avenues to the financial viability of microbial electrolysis cells [MEC] for domestic wastewater treatment and hydrogen production. Int. J. Hydrogen Energy 44 (5), 2426–2434.
Ambler, J.R., Logan, B.E., 2011. Evaluation of stainless steel cathodes and a bicarbonate buffer for hydrogen production in microbial electrolysis cells using a new method for measuring gas production. Int. J. Hydrogen Energy 36 (1), 160–166.
Belleville, P., Guillet, F., Pons, A., Deseure, J., Merlin, G., Druart, F., Ramousse, J., Grindler, E., 2018. Low voltage water electrolysis: Decoupling hydrogen production using bioelectrochemical system. Int. J. Hydrogen Energy 43 (32), 14867–14875.
Call, D.F., Wagner, R.C., Logan, B.E., 2009. Hydrogen production by *Geobacter* species and a mixed consortium in a microbial electrolysis cell. Appl. Environ. Microbiol. 75 (24), 7579–7587.
Call, D., Logan, B.E., 2008. Hydrogen production in a single chamber microbial electrolysis cell lacking a membrane. Environ. Sci. Technol. 42 (9), 3401–3406.
Cario, B., 2019. Evaluating the impact of substrate composition, reactor configuration, and operating conditions on the performance of bioelectrochemical systems treating fermentation effluents. Pennsylvania State University.
Cheng, S., Logan, B.E., 2011. Increasing power generation for scaling up single-chamber air cathode microbial fuel cells. Bioresour. Technol. 102 (6), 4468–4473.
Choi, M.-J., Yang, E., Yu, H.-W., Kim, I.S., Oh, S.-E., Chae, K.-J., 2019. Transition metal/carbon nanoparticle composite catalysts as platinum substitutes for bioelectrochemical hydrogen production using microbial electrolysis cells. Int. J. Hydrogen Energy 44 (4), 2258–2265.
Cotterill, S.E., Dolfing, J., Curtis, T.P., Heidrich, E.S., 2018. Community assembly in wastewater-fed pilot-scale microbial electrolysis cells. Front. Energy Res. 6.
Guo, H., Kim, Y., 2018. Scalable multi-electrode microbial electrolysis cells for high electric current and rapid organic removal. J. Power Sources 391, 67–72.
Hassanein, A., Witarsa, F., Guo, X., Yong, L., Lansing, S., Qiu, L., 2017. Next generation digestion: Complementing anaerobic digestion (AD) with a novel microbial electrolysis cell (MEC) design. Int. J. Hydrogen Energy 42 (48), 28681–28689.
Jafary, T., Daud, W.R.W., Ghasemi, M., Hong Kim, B., Bakar, M.H.A., Jahim, J.M., Ismail, M., Satar, I., Kamaruzzaman, M.A., 2017. Assessment of recirculation batch mode of operation in bioelectrochemical system; a way forward for cleaner production of energy and waste treatment. J. Clean Prod. 142, 2544–2555.
Jayabalan, T., Matheswaran, M., Naina Mohammed, S., 2018. Biohydrogen production from sugar industry effluents using nickel based electrode materials in microbial

electrolysis cell. Int. J. Hydrogen Energy. https://doi.org/10.1016/j.ijhydene.2018.09.219.
Jeremiasse, A.W., Hamelers, H.V.M., Saakes, M., Buisman, C.J.N., 2010. Ni foam cathode enables high volumetric H_2 production in a microbial electrolysis cell. Int. J. Hydrogen Energy 35, 12716–12723.
Jwa, E., Yun, Y.-M., Kim, H., Jeong, N., Park, S.-C., Nam, J.-Y., 2019. Domestic wastewater treatment in a tubular microbial electrolysis cell with a membrane electrode assembly. Int. J. Hydrogen Energy 44 (2), 652–660.
Kim, K.Y., Yang, W., Logan, B.E., 2018. Regenerable nickel-functionalized activated carbon cathodes enhanced by metal adsorption to improve hydrogen production in microbial electrolysis cells. Environ. Sci. Technol. 52 (12), 7131–7137.
Kim, K.-Y., Zikmund, E., Logan, B.E., 2017. Impact of catholyte recirculation on different 3-dimensional stainless steel cathodes in microbial electrolysis cells. Int. J. Hydrogen Energy 42 (50), 29708–29715.
Lalaurette, E., Thammannagowda, S., Mohagheghi, A., Maness, P.C., Logan, B.E., 2009. Hydrogen production from cellulose in a two-stage process combining fermentation and electrohydrogenesis. Int. J. Hydrogen Energy 34 (15), 6201–6210.
Li, F., Liu, W., Sun, Y., Ding, W., Cheng, S., 2017. Enhancing hydrogen production with Ni–P coated nickel foam as cathode catalyst in single chamber microbial electrolysis cells. Int. J. Hydrogen Energy 42 (6), 3641–3646.
Liu, H., Grot, S., Logan, B.E., 2005. Electrochemically assisted microbial production of hydrogen from acetate. Environ. Sci. Technol. 39 (11), 4317–4320.
Logan, B.E., 2008. Microbial Fuel Cells, 1 ed. Wiley, pp. 51–53.
Logan, B.E., Zikmund, E., Yang, W., Rossi, R., Kim, K.Y., Saikaly, P.E., Zhang, F., 2018. Impact of ohmic resistance on measured electrode potentials and maximum power production in microbial fuel cells. Environ. Sci. Technol.
Marcus, A.K., Torres, C.I., Rittman, B.E., 2010. Evaluating the impacts of migration in the biofilm anode using the model PCBIOFILM. Electrochim. Acta 55 (23), 6964–6972.
Miller, A., Singh, L., Wang, L., Liu, H., 2019. Linking internal resistance with design and operation decisions in microbial electrolysis cells. Environ. Int. 126, 611–618.
Nam, J.-Y., Logan, B.E., 2012. Optimization of catholyte concentration and anolyte pHs in two chamber microbial electrolysis cells. Int. J. Hydrogen Energy 37 (24), 18622–18628.
Rago, L., Baeza, J.A., Guisasola, A., 2016. Increased performance of hydrogen production in microbial electrolysis cells under alkaline conditions. Bioelectrochemistry 109, 57–62.
Rossi, R., Cario, B.P., Santoro, C., Yang, W., Saikaly, P., Logan, B.E., 2019. Evaluation of electrode and solution area-based resistances enables quantitative comparisons of factors impacting microbial fuel cell performance. Environ. Sci. Technol. 53 (7), 3977–3986. https://doi.org/10.1021/acs.est.8b06004.
Roubaud, E., Lacroix, R., Da Silva, S., Bergel, A., Basseguy, R., Erable, B., 2018. Catalysis of the hydrogen evolution reaction by hydrogen carbonate to decrease the voltage of microbial electrolysis cell fed with domestic wastewater. Electrochim. Acta 275, 32–39.
Rozendal, R.A., Hamelers, H.V.M., Euverink, G.J.W., Metz, S.J., Buisman, C.J.N., 2006. Principle and perspectives of hydrogen production through biocatalyzed electrolysis. Int. J. Hydrogen Energy 31, 1632–1640.
Rozendal, R.A., Hamelers, H.V., Molenkamp, R.J., Buisman, C.J., 2007. Performance of single chamber biocatalyzed electrolysis with different types of ion exchange membranes. Water Res. 41 (9), 1984–1994.
Sleutels, T.H.J.A., Hamelers, H.V.M., Rozendal, R.A., Buisman, C.J.N., 2009a. Ion transport resistance in Microbial Electrolysis Cells with anion and cation exchange membranes. Int. J. Hydrogen Energy 34, 3612–3620.
Sleutels, T.H.J.A., Lodder, R., Hamelers, H.V.M., Buisman, C.J.N., 2009b. Improved performance of porous bio-anodes in microbial electrolysis cells by enhancing mass and charge transport. Int. J. Hydrogen Energy 34, 9655–9661.
Torres, C.I., Kato Marcus, A., Rittmann, B.E., 2008. Proton transport inside the biofilm limits electrical current generation by anode-respiring bacteria. Biotechnol. Bioeng. 100 (5), 872–881.
Ullery, M.L., Logan, B.E., 2015. Anode acclimation methods and their impact on microbial electrolysis cells treating fermentation effluent. Int. J. Hydrogen Energy 40 (21), 6782–6791.
Wang, A., Sun, D., Cao, G., Wang, H., Ren, N., Wu, W.M., Logan, B.E., 2011. Integrated hydrogen production process from cellulose by combining dark fermentation, microbial fuel cells, and a microbial electrolysis cell. Bioresour. Technol. 102 (5), 4137–4143.
Wang, H., Ren, Z.J., 2013. A comprehensive review of microbial electrochemical systems as a platform technology. Biotechnol. Adv. 31 (8), 1796–1807.
Wang, Y.-Z., Zhang, L., Xu, T., Ding, K., 2017. Influence of initial anolyte pH and temperature on hydrogen production through simultaneous saccharification and fermentation of lignocellulose in microbial electrolysis cell. Int. J. Hydrogen Energy 42 (36), 22663–22670.
Watson, V.J., Delgado, C.N., Logan, B.E., 2013. Influence of chemical and physical properties of activated carbon powders on oxygen reduction and microbial fuel cell performance. Environ. Sci. Technol. 47 (12), 6704–6710.
Yang, W., Kim, K.-Y., Saikaly, P.E., Logan, B.E., 2017. The impact of new cathode materials relative to baseline performance of microbial fuel cells all with the same architecture and solution chemistry. Energy Environ. Sci. 10, 1025–1033.
Yang, W., Logan, B.E., 2016. Immobilization of a metal–nitrogen–carbon catalyst on activated carbon with enhanced cathode performance in microbial fuel cells. ChemSusChem 9, 16.
Yu, Z., Leng, X., Zhao, S., Ji, J., Zhou, T., Khan, A., Kakde, A., Liu, P., Li, X., 2018. A review on the applications of microbial electrolysis cells in anaerobic digestion. Bioresour. Technol. 255, 340–348.
Zhang, F., Liu, J., Ivanov, I., Hatzell, M.C., Yang, W., Ahn, Y., Logan, B.E., 2014. Reference and counter electrode positions affect electrochemical characterization of bioanodes in different bioelectrochemical systems. Biotechnol. Bioeng. 111 (10), 1931–1939.
Zikmund, E., Kim, K.-Y., Logan, B.E., 2018. Hydrogen production rates with closely-spaced felt anodes and cathodes compared to brush anodes in two-chamber microbial electrolysis cells. Int. J. Hydrogen Energy 43 (20), 9599–9606.